

# Learn to Ignore: Domain Adaptation for Multi-Site MRI Analysis

**Julia Wolleb<sup>1</sup>, Robin Sandkühler<sup>1</sup>, Florentin Bieder<sup>1</sup>, Muhamed Barakovic<sup>1</sup>, Athina Papadopoulou<sup>1,2</sup>, Nouchine Hadjikhani<sup>3,4</sup>, Özgür Yaldizli<sup>1,2</sup>, Jens Kuhle<sup>2</sup>, Cristina Granziera<sup>1,2</sup>, Philippe C. Cattin<sup>1</sup>**

<sup>1</sup> Department of Biomedical Engineering, University of Basel, Allschwil, Switzerland

<sup>2</sup> University Hospital Basel, Switzerland

<sup>3</sup> Gillberg Neuropsychiatry Center, Sahlgrenska Academy, University of Gothenburg, Sweden

<sup>4</sup> Massachusetts General Hospital, Harvard Medical School, Charlestown, Massachusetts, United States of America

julia.wolleb@unibas.ch

## Abstract

Limited availability of large image datasets is a major issue in the development of accurate and generalizable machine learning methods in medicine. The limitations in the amount of data are mainly due to the use of different acquisition protocols, different hardware, and data privacy. At the same time, training a classification model on a small dataset leads to a poor generalization quality of the model. To overcome this issue, a combination of various image datasets of different provenance is often used, e.g., multi-site studies. However, if an additional dataset does not include all classes of the task, the learning of the classification model can be biased to the device or place of acquisition. This is especially the case for Magnetic Resonance (MR) images, where different MR scanners introduce a bias that limits the performance of the model. In this paper, we present a novel method that learns to ignore the scanner-related features present in the images, while learning features relevant for the classification task. We focus on a real-world scenario, where only a small dataset provides images of all classes. We exploit this circumstance by introducing specific additional constraints on the latent space, which lead the focus on disease-related rather than scanner-specific features. Our method *Learn to Ignore* outperforms state-of-the-art domain adaptation methods on a multi-site MRI dataset on a classification task between Multiple Sclerosis patients and healthy subjects.<sup>1</sup>

## 1 Introduction

Magnetic Resonance Imaging (MRI) is an imaging modality that is often used in the daily clinical routine. Due to its high soft-tissue contrast, it is a powerful diagnostic tool for many neurological disorders, e.g., tumors, stroke, and neurodegenerative or neuroinflammatory diseases such as dementia and Multiple Sclerosis (MS). Different soft-tissue contrasts can be achieved by using different MR sequences, e.g., T1-weighted, T2-weighted, or FLAIR. MRI is thereby able to visualize different characteristics present in the brain tissue and provide valuable information to the physician.

<sup>1</sup>This work has been submitted to the IEEE for possible publication. Copyright may be transferred without notice, after which this version may no longer be accessible.

Compared to other imaging modalities like computed tomography, MR images only provide relative values for different tissue types. These relative values often depend on the scanner manufacturer, the scan protocol or even the software version. This means that two scans of the same subject, acquired with the same magnetic field strength, the same MR sequence, but with different hardware and software, can result in different values for the same type of tissue characteristics. We refer to this problem as the scanner bias. While human medical experts can adapt to those relative changes, they represent a major problem for machine learning methods. Although state-of-the-art methods could handle the scanner bias if enough training data for all the different MR settings would be available, creating such an extensive image database is very challenging. Furthermore, the features that are related to the scanner bias are often more prominent and distract from other features related to the actual task, e.g., disease-related features. Consequently, the focus lies only on features related to the scanner bias, and this leads to a low generalization quality of the model.

In the literature, these kind of problems are known as *domain adaptation problems* (Ben-David et al. 2010). In the scope of machine learning, one can define domain adaptation as learning a main task from a *source domain*. The learned model then should perform well on a different *target domain*. It thereby has to overcome the domain shift between the source domain and the target domain. Examples of domain adaptation include digit recognition (Rozantsev, Salzmann, and Fua 2018), road scene segmentation (Zhang, David, and Gong 2017) and face recognition tasks (Wen et al. 2018).

**Related Work** The problem of using images from different MR scanners can be tackled with domain transfer, where images are translated from one domain to another (Wolterink et al. 2017). DeepHarmony (Dewey et al. 2019) uses paired data to change the contrast of MRI from one scanner to another scanner with a modified U-Net. Generative Adversarial Networks (Huang et al. 2018; Sankaranarayanan et al. 2018; Lei et al. 2019; Wang, Zhang, and Fu 2020) aim to generate new images to overcome the domain shift. Those methods modify the intensities of each pixel before train-

ing for the main task. This approach is preferably avoided in medical applications, as it bears the risk of removing important pixel level information required later for other tasks, such as segmentation or anomaly detection.

Several domain adaption methods have been presented to overcome MR scanner related issues. One can generally distinguish between unsupervised domain adaptation (UDA) (Tzeng et al. 2017; Perone et al. 2019), where the target domain data is unlabeled, or supervised domain adaptation (SDA)(Tzeng et al. 2015; Kushibar et al. 2019), where the labels of target domain are used during training. UDA can be used for multi-site segmentation of MS lesions from MRI (Ackaouy et al. 2020). Furthermore, extensive data augmentation of MR images has been shown to improve segmentation results (Novosad, Fonov, and Collins 2019; Bilot et al. 2020). Another UDA approach, based on domain-adversarial neural networks (Ganin et al. 2016), is used for multi-site brain lesion segmentation (Kamnitsas et al. 2017). Several SDA approaches have been proposed for MRI classification or segmentation (Hosseini-Asl, Keynton, and El-Baz 2016; Valverde et al. 2019; Kaur et al. 2019). Unlearning the scanner bias (Dinsdale, Jenkinson, and Namburete 2020) is an SDA method for MRI harmonisation and manages to improve the performance in age prediction from MR images.

The introduction of contrastive loss terms (Khosla et al. 2020; Wen et al. 2016; Schroff, Kalenichenko, and Philbin 2015; Hadsell, Chopra, and LeCun 2006) can also be used for domain generalization (Kang et al. 2019; Park et al. 2020; Motiian et al. 2017; Dou et al. 2019; Chaitanya et al. 2020). Fine-tuning of classification networks can be done by manipulating the feature representations of the input images (Hinterreiter, Streit, and Kainz 2020). Disentangling the latent space has also previously been done for MRI harmonization (Chartsias et al. 2019; Dewey et al. 2020). In (Ma et al. 2018) the problem of classifying multi-site MR images is tackled with multi-task learning.

**Problem Statement** All the methods mentioned above have in common that they must be able to learn the main task from the source domain. In contrast to them, we tackle a new supervised domain adaptation problem that frequently occurs in real-world applications. This problem focuses on the bias present in datasets of various provenance, which disturbs the learning of a specific task. Due to the high variability in data, often only a small and specific dataset is at hand to learn a main task. Training on this dataset alone yields a low generalization quality of the model. Using additional datasets of other provenance can be problematic due to the bias between the datasets. Figure 1 illustrates the problem and the relation of the different datasets for the task of binary classification.

Here, Dataset 1 forms the target domain with a small number of training samples of class 1 and class 2. In order to increase the number of training samples, we add the Datasets 2-6. These additional datasets of various provenance, e.g., different MR scanners, define the source domain. It can happen that the additional datasets only provide images of either class 1 or class 2. This problem has practi-

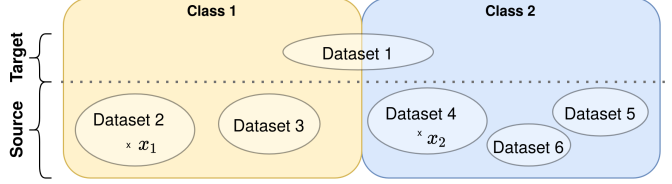


Figure 1: Quantity chart for the datasets in the source and target domain. Only Dataset 1 contains images of both classes, this forms the target domain. All the other datasets constitute the source domain.

cal relevance in the clinic, especially regarding MR datasets: Already small changes in the acquisition protocol induce a scanner bias. Therefore it gets extremely difficult to collect large databases with the same acquisition settings, even within the same hospital. Moreover, often only data of diseased subjects is collected. The dataset needs to be amended with healthy subjects from other unrelated studies, resulting in the problem presented in Figure 1.

The challenge of such a setup is that during training, the classification networks tend to focus on provenance-inherent rather than task specific features. For example, given two images from the source domain, exemplary image  $x_1$  belongs to class 1 and originates from Dataset 2. Another image  $x_2$  belongs to class 2 and originates from Dataset 4. When the model needs to assign a class label to  $x_1$ , it can just take features related to Dataset 2 into account. The model tends to cheat by learning *dataset-related features* rather than *class-specific features* to classify  $x_1$  and  $x_2$ . Using a standard classification loss, the model is not penalized for taking the wrong features into account during training on the source domain. Consequently, the main task cannot be learned from the source domain alone, which results in a poor generalization quality of the model. When learning the domain shift between source and target domain with a classical domain adaptation approach, the model will show a poor performance on the target domain, since it learned the wrong task on the source domain.

To the best of our knowledge, there is no other work that presented a solution for this specific real-world problem. Our problem differs substantially from classical domain adaptation or contrastive learning problems, where the main task is learned on the source domain alone.

In this work, we present a new method called *Learn to Ignore (L2I)*, which learns to ignore the described provenance-related features that result in a poor generalization quality of the model. We exploit the fact that the target domain contains images of subjects of all classes with the same provenance, and use this dataset to lead the model’s attention to task specific features. We developed specific constraints on the latent space and introduce two novel loss terms that can be added to any classification network. We evaluate our method on a multi-site MR dataset of Multiple Sclerosis patients and healthy subjects. Our method aims to ignore features related to the scanner bias while focusing on disease-related features for classification between healthy and diseased subjects. We compare *L2I* to state-of-the-art methods

on the MS cohort dataset, and perform various ablation studies of our method. The corresponding results on the Office31 dataset for classical domain adaptation can be found in Section 1 of the technical appendix.

## 2 Method

We developed a strategy that aims to ignore features that disturb the learning of a classification task between  $n$  classes. The building blocks of our setup are shown in Figure 2. The input image  $x_i \in \mathbb{R}^3$  of class  $i \in \{1, \dots, n\}$  is the input for the encoder network  $E$  with parameters  $\theta_E$ . This encoder network follows the structure of the encoder of Inception-Resnet-v1 (Szegedy et al. 2017). However, we replaced the 2D convolutions with 3D convolutions and changed the batch normalization layers to instance normalization layers, because memory restrictions limit the batch-size when using 3D input data. The output is the latent vector  $f_i = E(x_i) \in \mathbb{R}^m$ , where  $m$  denotes the dimension of the latent space. This latent vector is normalized to a length of 1 and forms the input for the classification network  $C$  with parameters  $\theta_C$ . Finally, we get the classification scores  $p_i = C(f_i) = C(E(x_i))$  for class  $i \in \{1, \dots, n\}$ . To make the separation between the classes in the latent space learnable, we introduce additional learnable parameters  $\theta_O$  that learn normalized center points  $\mathcal{O} = \{o_1, \dots, o_n\} \subset \mathbb{R}^m$ . To suppress the scanner-related features, we want to embed the latent vectors in the latent space in such a way that latent vectors from the same class are close to each other while those from different classes are further apart. This property should hold irrespective of the domain. To achieve this, we exploit the fact that the target domain contains images of all classes of the same provenance. The model learns the separation of the embeddings using data of the target domain only. Consequently, no provenance-inherent feature can be used to determine the center points of the different classes and the model learns to focus on class-specific features. We force the latent vector  $f_i$  of an input image  $x_i$  into a hypersphere of radius  $r$  centered in  $o_i$ . Those center points  $o_i$  lie on the unit hypersphere and should have a distance larger than  $d$  from each other. A schematic overview in 2D for the case of  $n = 2$  classes is given in Figure 3.

We denote the latent vector of an image of the target domain of class  $i$  as  $f_{i,t}$ , where  $t$  denotes the affiliation to the target domain. The center points  $\mathcal{O}$  are learned considering the latent vectors  $f_{i,t}$ . This means that  $o_i \in \mathcal{O}$  is learned using  $f_{i,t}$ , such that  $o_i$  is close to  $f_{i,t}$ , for  $i \in \{1, \dots, n\}$ , and  $o_i$  is far from  $o_j$  for  $i \neq j$ . With this setup, the center points are learned and separated from each other using data only from the target domain. A strength of our method is that one can freely add more datasets of new provenance to the source domain, without any need to alter the method, even if the new datasets contain images of only one class. This gives a bigger flexibility and can be very helpful when there is a need to increase the amount of training data. This is especially valuable for clinical applications, as it gives the possibility to include data from other unrelated studies, e.g., a large dataset of healthy controls and publicly available data. Our method can be generally integrated in other network architectures on different datasets for other tasks.

## 2.1 Loss functions

The overall objective function is given by

$$\mathcal{L}_{\text{total}} = \underbrace{\lambda_{\text{cls}} \mathcal{L}_{\text{cls}}}_{\theta_C} + \underbrace{\lambda_{\text{center}} \mathcal{L}_{\text{center}}}_{\theta_O, \theta_E} + \underbrace{\lambda_{\text{latent}} \mathcal{L}_{\text{latent}}}_{\theta_E}. \quad (1)$$

It consists of three components: A classification loss  $\mathcal{L}_{\text{cls}}$ , a center point loss  $\mathcal{L}_{\text{center}}$  for learning  $\mathcal{O} = \{o_1, \dots, o_n\}$ , and a loss  $\mathcal{L}_{\text{latent}}$  on the latent space. Those components are weighted with the hyperparameters  $\lambda_{\text{cls}}, \lambda_{\text{latent}}, \lambda_{\text{center}} \in \mathbb{R}$ . The parameters  $\theta_E, \theta_C$  and  $\theta_O$  indicate what parameters of the network are updated with what components of the loss term. With this total loss objective, any classification network can be extended by our method.

**Classification Loss** The classification loss is defined by the cross-entropy loss:

$$\mathcal{L}_{\text{cls}, \theta_C}(f_i) = - \sum_{k=1}^n \mathbb{1}_{k=i} \log(p_k). \quad (2)$$

We want to point out that the gradient is only calculated with respect to  $\theta_C$ . For this reason, only the parameters  $\theta_C$  are updated with this loss term. If we would also update the parameters  $\theta_E$  with this loss term, the training would be disturbed by the scanner bias, just like in the training of a vanilla classifier, see Section 4 for more details.

**Center Point Loss** We designed a novel loss function to determine the center points. It is defined by the distance from a latent vector  $f_{i,t}$  of the target domain to its corresponding center point  $o_i$ . Moreover,  $o_i$  and  $o_j$  should be far enough from each other for  $i \neq j$ . Just like the latent vectors,  $o_i$  is also normalized to a length of one. Therefore, the maximal possible distance between  $o_i$  and  $o_j$  equals 2. We define a radius  $r > 0$  and force the latent vectors of the target domain  $f_{i,t}$  to be within a hypersphere of radius  $r$  centered in  $o_i$ . Furthermore, we define a distance  $d$  with  $2r < d < 2$ , and add a loss term forcing the distance between  $o_i$  and  $o_j$  to be larger than  $d$ .

The choice of  $d$  and  $r$  is closely related to the choice of a margin in conventional contrastive loss terms (Schroff, Kalenichenko, and Philbin 2015; Hadsell, Chopra, and Le-Cun 2006). By choosing  $d < 2$  and  $r > 0$  with  $d > 2r$ , the network is not penalized for not forcing  $o_i$  in the perfect position, but only to an acceptable region, such that the hyperspheres do not overlap. Then, the center point loss used to update the parameters  $\theta_O$  and  $\theta_E$  is given by

$$\begin{aligned} \mathcal{L}_{\text{center}, \theta_O, \theta_E}(f_{i,t}, \mathcal{O}) = & \sum_{k=1}^n \mathbb{1}_{k=i} \left( \max(\|f_{k,t} - o_k\|_2 - r, 0)^2 \right. \\ & \left. + \sum_{j \neq k} \frac{1}{2} \max(d - \|o_k - o_j\|_2, 0)^2 \right). \end{aligned} \quad (3)$$

**Latent Loss** We define the loss on the latent space, similar to the *Center Loss* (Wen et al. 2016), by the distance from

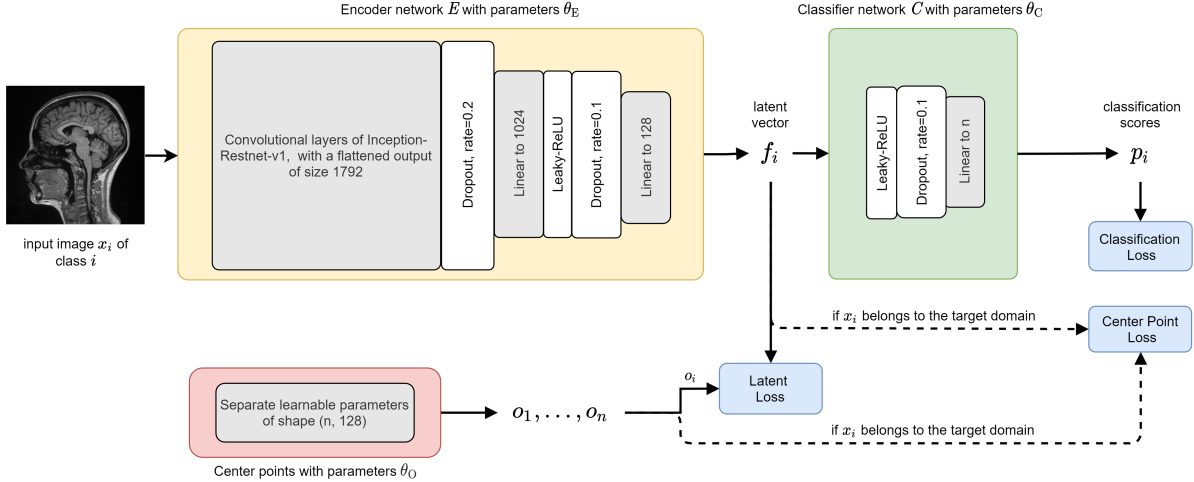


Figure 2: Architecture of the classification network consisting of an encoder  $E$  with parameters  $\theta_E$ , a fully connected classifier  $C$  with parameters  $\theta_C$ , and separate learnable parameters  $\theta_O$ . Here,  $o_1, \dots, o_n$  are learnable center points in the latent space,  $f_i$  is a vector in the latent space, and  $p_i$  is the classification score for class  $i$ . The loss components are shown in blue.

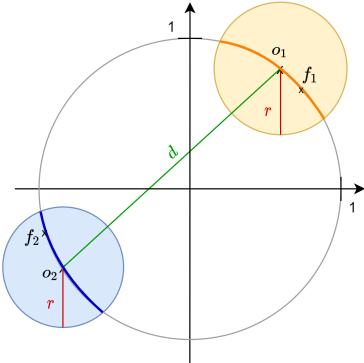


Figure 3: The diagram shows a 2D sketch of the proposed latent space for  $n = 2$  classes, with two learnable center points  $o_1$  and  $o_2$ . The latent vectors are normalized and lie on the unit hypersphere denoted by the grey circle. The goal is that latent vectors  $f_1$  of images of class 1 lie within the yellow circle on the orange line, and latent vectors  $f_2$  of images of class 2 lie within the blue circle on the blue line.

$f_i$  to its corresponding center point  $o_i$ . The latent loss is thus defined as

$$\mathcal{L}_{\text{latent}, \theta_E}(f_i, \mathcal{O}) = \sum_{k=1}^n \mathbb{1}_{k=i} \max(\|f_i - o_k\|_2 - r, 0)^2. \quad (4)$$

With this loss, all latent vectors  $f_i$  of the training set of class  $i$  are forced to be within a hypersphere of radius  $r$  around the center point  $o_i$ . This loss is used to update the parameters  $\theta_E$  of the encoder. By choosing  $r > 0$ , the network is given some leeway to force  $f_i$  to an acceptable region around  $o_i$ , denoted by the orange and blue lines in Figure 3.

### 3 Experiments

We apply our method *L2I* to a multi-site MRI dataset with MS patients and healthy subjects for binary classification. Experiments on the Office31 dataset (Saenko et al. 2010) for classical domain adaptation can be found in Section 1 of the technical appendix.

#### 3.1 Training Details

We train our model with the Adam optimizer (Kingma and Ba 2014) with  $\beta_1 = 0.9$ ,  $\beta_2 = 0.999$  and a weight decay of  $5 \cdot 10^{-5}$ . The learning rate for the parameters  $\theta_O$  is  $lr_O = 10^{-4}$ , while the learning rate for the parameters  $\theta_C$  and  $\theta_E$  is  $lr_{E,C} = 5 \cdot 10^{-5}$ . The weights of the loss components are manually chosen as  $\lambda_{\text{cls}} = 1$ ,  $\lambda_{\text{latent}} = 1$ , and  $\lambda_{\text{center}} = 100$ . Furthermore, we empirically choose the distance  $d = 1.9$  and the radius  $r = 0.1$ .

An early stopping criterion, with a patience value of 20, based on the validation loss on the target domain is used to stop the training. For data sampling in the training set, we use the sampling scheme presented in Algorithm 1. Data augmentation includes rotation, gamma correction, flipping, scaling and cropping. The training was performed on a NVIDIA Quadro RTX 6000 GPU.

---

#### Algorithm 1: Sampling scheme

---

**repeat**

- Sample a random batch from the whole training set (target and source domain) of size 10. Use this batch to calculate  $\mathcal{L}_{\text{cls}}$  and  $\mathcal{L}_{\text{latent}}$ .
- Sample one image from the target domain of each class and calculate  $\mathcal{L}_{\text{center}}$ .
- Update network parameters with  $\mathcal{L}_{\text{total}}$ .

**until** early stopping criterion on validation loss is reached.

---

### 3.2 Multiple Sclerosis Dataset

In this project, the main task is to distinguish between patients suffering from MS and subjects of a healthy control group. All images are T1-weighted images taken from many different 3T MR scanners with the MPRAGE sequence. The quantity chart in Figure 4 visualizes the different allocations of the MS dataset.

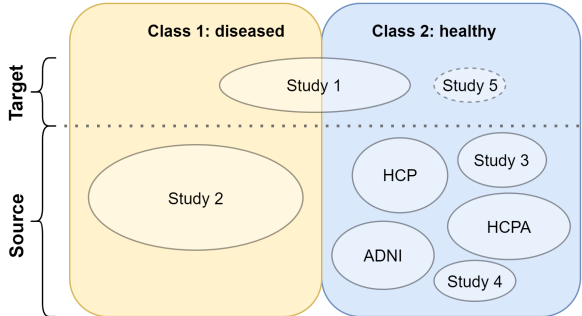


Figure 4: Data affiliation of the MS dataset. Only the monocentric study 1 contains images of both classes, forming the target domain. For validation, study 1 is supplemented with study 5. All the other studies form the source domain.

We collect images from five different in-house studies. For data privacy concerns, this patient data is not publicly available. Written informed consent was obtained from all subjects enrolled in the studies. All data were coded (i.e. pseudoanonymized) at the time of the enrolment of the patients. Those studies differ in scanner hardware, scanning protocol or software version. We refer to this as the scanner bias, due to which the studies are treated as separate datasets. Only Study 1 provides us with images of both healthy and diseased subjects acquired on the same scanner with the same settings. We denote this dataset as the *target domain*. This target domain alone, however, does not yield enough data to learn the main task. Since there are only very few images of healthy subjects in Study 1, we add 9 images of healthy subjects of the in-house Study 5. Those images were also acquired on the same scanner, but they differ in the acceleration factor from images of Study 1. To make sure that this slight difference does not disturb the training or provide biased results during test time, we use those images only for validation.

In clinical studies, the number of images of patients and healthy controls is often not balanced. This also holds for our in-house studies. To overcome this, we add healthy controls from publicly available datasets: We also use MPRAGE images from the Alzheimer’s Disease Neuroimaging Initiative<sup>2</sup> (ADNI) dataset, the Young Adult Human Connectome Project<sup>3</sup> (HCP) (Van Essen et al. 2012) and the Human Connectome Project - Aging (HCPA) (Harms et al. 2018).

<sup>2</sup>Data used in preparation of this article were obtained from the Alzheimer’s Disease Neuroimaging Initiative(ADNI) database (adni.loni.usc.edu). The investigators within the ADNI contributed to the design and implementation of ADNI and/or provided data but did not participate in analysis or writing of this report.

<sup>3</sup>Data were provided by the Human Connectome Project, WU-

A summary of the number of images of the different studies is given in Table 1, including the split into training, validation and test set. More information about the scanner models and subjects of the different datasets can be found in Section 2 of the technical appendix.

All images were preprocessed using the same pipeline consisting of skull-stripping with HD-bet (Isensee et al. 2019), N4 biasfield correction (Tustison et al. 2010), resampling to a voxel size of  $1 \times 1 \times 1 \text{ mm}^3$ , cutting the top and lowest two percentiles of the pixel intensities, and finally an affine registration to the MNI 152 standard space<sup>4</sup>. All images are cropped to a size of (124, 120, 172). Although this preprocessing pipeline increases the similarity between the images to some extend, the scanner bias still has a big impact. Figure 5 shows an example of the scanner bias effect for two healthy control groups of the ADNI and HCP dataset. It can clearly be seen that the distribution of the pixel intensities is still different for each dataset after the preprocessing, while using the same MR sequence. This difference originates from variations in scanner hardware, software version or scanning protocols. Histogram matching is not taken into account here, because we want to preserve the original contrasts of the images for future work.

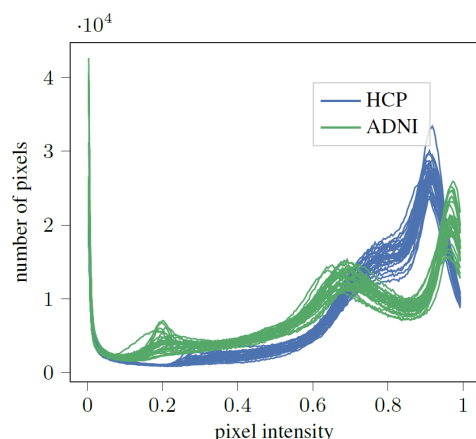


Figure 5: Distribution of the pixel intensities for preprocessed and normalized MPRAGE MR images of healthy subjects of the ADNI and the HCP dataset.

As can be seen in Table 1, the training set mainly consist of data from the source domain, where all the studies provide either healthy or diseased subjects. Therefore, during training of a classification network, there is the risk that the network learns scanner-related rather than disease-specific features. Training of *L2I* takes about 8 hours on this dataset.

Minn Consortium (Principal Investigators: David Van Essen and Kamil Ugurbil; 1U54MH091657) funded by the 16 NIH Institutes and Centers that support the NIH Blueprint for Neuroscience Research; and by the McDonnell Center for Systems Neuroscience at Washington University.

<sup>4</sup>Copyright 1993-2009 Louis Collins, McConnell Brain Imaging Centre, Montreal Neurological Institute, McGill University

		TRAINING SET		VALIDATION SET		TEST SET	
		HEALTHY	DISEASED	HEALTHY	DISEASED	HEALTHY	DISEASED
TARGET	STUDY 1	16	55	9	9	15	15
	STUDY 5						
SOURCE	STUDY 2	368		20		30	
	ADNI	113		6		9	
	HCP	89		4		7	
	HCPA	140		7		10	
	STUDY 3	40		2		3	
	STUDY 4	22		1		1	

Table 1: Overview of the studies in the MS dataset. The dataset is split proportionally into training, validation and test set. All images are T1-weighted MPRAGE images acquired with a 3T MR scanner.

## 4 Results and Discussion

To measure the classification performance, we calculate the classification accuracy (Acc), the Cohen’s kappa score (Cohen 1960) and the area under the receiver operating characteristic curve (AUROC) (Hanley and McNeil 1982). We compare ourselves against the following listed methods. Implementation details of all comparing methods can be found in the supplementary material. The method *Vanilla* and its extensions *Class-aware* and *Weighted* are first trained on the target domain only, keeping the same train/validation/test split as shown in Table 1, and then also on the source and the target domain as described in Table 1. The other methods are trained on the source and the target domain. The methods *Fixed* and *No-margin* are ablation studies of *L2I*.

- **Vanilla classifier (*Vanilla*):** This classifier follows the same architecture as *L2I*, but only  $\mathcal{L}_{cls}$  is taken to update the parameters of both the encoder and classifier.
- **Class-aware Sampling (*Class-aware*):** We train the *Vanilla* classifier with  $\mathcal{L}_{cls}$  and use class-aware sampling. When training on the target domain only, we sample such that in every batch, there are 5 images for each class. When training on both the source and the target domain, we make sure that in every batch, there is at least one example from both classes and both domains. We sample in a way that in every batch, there are 5 images from the source domain for each class, and 1 image from the target domain for each class. This is similar to the sampling scheme of the *CAN* and the *Unlearning* method.
- **Weighted Loss (*Weighted*):** We train the *Vanilla* classifier with  $\mathcal{L}_{cls}$  and introduce weights to the loss function to compensate for class imbalances. When training on the target domain alone, we group the input images according to their class, resulting in two groups. When training on both the source and the target domain, we group the input images according to their domain and class, resulting in four groups. The loss is weighted according to the inverted proportion of the group in the whole training set.
- **Domain-Adversarial Neural Network (*DANN*)** (Ganin et al. 2016): The classifier learns both to distinguish between the domains and between the classes. It includes a gradient reversal for the domain classification.

- **Unlearning Scanner Bias (*Unlearning*)** (Dinsdale, Jenkinson, and Namburete 2020): Like in the *DANN* method, the classifier learns to predict the domain. It is also trained to classify between the classes, which is the main task. A confusion loss aims to maximally confuse the domain predictor, such that only features relevant for the main task are extracted.
- **Supervised Contrastive Learning (*Contrastive*)** (Khosla et al. 2020): This state-of-the-art method takes the latent vectors into account and tries to push them into clusters far apart from each other, with a sampling scheme and a contrastive loss term allowing for multiple positives and negatives per input image. This loss formulation maximizes a lower bound on mutual information (Oord, Li, and Vinyals 2018).
- **Contrastive Adaptation Network (*CAN*)** (Kang et al. 2019): To the best of our knowledge, this combination of taking the maximum mean discrepancy of the latent vectors as loss objective, class-aware sampling and clustering is currently the leader for domain adaptation on the Office31 dataset.
- **Fixed Center Points (*Fixed*):** In our case of binary classification, we train *L2I*, but instead of learning the centerpoints  $o_1$  and  $o_2$  using the target domain, we fix the center points at 
$$o_i = \frac{v_i}{\|v_i\|_2} \text{ for } i \in \{1, 2\}, \text{ with } v_1 = (1, \dots, 1) \text{ and } v_2 = (-1, \dots, -1).$$
- **No margin (*No-margin*):** In our case of binary classification, we train *L2I* with  $d = 2$  and  $r = 0$ , such that no margin is chosen in the Contrastive Loss term in Equations 3 and 4.

### 4.1 Results on the MS Dataset

We report the mean and standard deviation of 10 runs, where for each run the dataset is randomly divided into training, validation and test set as described in Table 1. In Table 3, the results for *Vanilla*, *Class-aware* and *Weighted* are shown when only data of the target domain is taken into account. The very poor performance is due to the fact that training on such a small dataset leads to overfitting and a poor generalization quality of the model. Therefore, the target do-

	TARGET DOMAIN			SOURCE DOMAIN		
	ACC	KAPPA	AUROC	ACC	KAPPA	AUROC
VANILLA	69.0 [6.1]	38.0 [12.1]	79.8 [7.3]	90.3 [5.7]	80.7 [11.3]	95.0 [5.9]
· CLASS-AWARE	71.0 [8.3]	42.0 [16.6]	79.3 [13.3]	90.7 [4.2]	81.3 [8.3]	95.3 [3.9]
· WEIGHTED	71.3 [6.3]	42.7 [12.7]	81.2 [7.8]	92.2 [3.1]	84.6 [6.3]	95.1 [3.4]
DANN	67.0 [5.7]	34.0 [11.5]	74.7 [8.4]	93.1 [2.8]	86.3 [5.5]	98.7 [0.7]
UNLEARNING	70.7 [6.6]	41.3 [13.3]	81.7 [9.2]	85.5 [3.2]	71.0 [6.5]	90.5 [3.3]
CONTRASTIVE	76.3 [6.7]	52.6 [13.5]	86.7 [9.5]	<b>94.5 [2.4]</b>	<b>89.0 [4.7]</b>	<b>98.9 [0.7]</b>
CAN	75.3 [6.9]	50.7 [13.8]	83.8 [8.8]	92.8 [2.5]	85.7 [5.0]	96.7 [1.8]
L2I [OURS]	<b>89.0 [3.9]</b>	<b>78.0 [7.7]</b>	<b>89.7 [7.6]</b>	92.0 [2.5]	84.0 [4.9]	91.7 [4.9]
· FIXED	71.7 [7.2]	43.3 [14.5]	76.5 [11.4]	90.5 [3.9]	81.0 [7.9]	90.2 [5.8]
· NO-MARGIN	82.0 [3.9]	64.0 [7.8]	75.3 [9.1]	91.7 [4.8]	83.3 [9.7]	84.9 [3.9]

Table 2: Mean [standard deviation] of the classification results for the various methods on the test set, when trained and evaluated on the target and on the source domain for 10 runs. Our method *L2I* is the only one that achieves good results on the target domain, without loss of performance on the source domain.

	ACC	KAPPA	AUROC
VANILLA	50.0 [0.0]	0.0 [0.0]	59.5 [13.0]
· CLASS-AWARE	65.0 [5.0]	29.3 [9.5]	68.6 [12.4]
· WEIGHTED	50.3 [1.1]	0.0 [0.0]	73.3 [13.5]

Table 3: Mean [standard deviation] of the classification results for the *Vanilla*, *Class-aware* and *Weighted* methods when trained only on the target domain for 10 runs.

main needs to be supplemented with more data from other datasets. In Table 2, the classification results for the various methods presented in Section 4 when trained on the whole MS dataset are summarized. The high values for the standard deviations are also due to the small number of samples in the test set: Already a different classification of one image leads to a high difference in the classification score. Our method *L2I* strongly outperforms all other methods on the target domain. Although we favour the target domain during training by learning  $o_1$  and  $o_2$  accordingly, we see that *L2I* still has a good performance on the source domain. Therefore, we claim that the model learned to distinguish the classes based on disease-related features that are present in both target and source domain, rather than scanner-related features.

The benefit of learning  $o_1$  and  $o_2$  by taking only the target domain into account can be seen when comparing our method against *Fixed*, where the center points are fixed. The problem of fixed center points is that during training, the model can still take provenance-inherent features to move the latent vector  $f_i$  to the corresponding center point  $o_i$ , and features belonging to the main task are suppressed. Moreover, comparing *L2I* to *No-margin*, we can see that choosing  $d < 2$  and  $r > 0$  brings an advantage.

All methods perform well on the source domain. This is due to the special situation in our dataset, where scanner-related features can be taken into account for classification on the source domain. However, this leads to a poor performance of the *Vanilla* classifier on the target domain, where only disease-related features can be used. Also the extensions to the *Vanilla* classifier, *Class-aware* and *Weighted*, cannot

drastically lift its performance level. A visualization of the comparison between the *Vanilla* classifier and our method *L2I* can be found in the t-SNE plots in Section 3 of the technical appendix.

In this setup, the domain adaptation or contrastive learning methods *DANN* and *Contrastive*, as well as the state-of-the-art methods *CAN* and *Unlearning* fail to show the performance they have on classical domain adaptation problems. They face the issue that they are not able to learn the main task from the source domain, as is proposed in their original setups. Therefore, classical domain adaptation and contrastive learning methods do not provide a solution for our specific problem.

## 5 Conclusion

In this work, we presented a method that is able to ignore image features that are induced by different MR scanners. We design specific constraints on the latent space and define two novel loss terms, which can be added to any classification network. The novelty lies in learning the center points in the latent space using images of the target domain. Consequently, the separation of the latent space can only be learned based on task-specific features, also in cases where the main task cannot be learned from the source domain alone. Our problem therefore differs substantially from classical domain adaptation or contrastive learning problems.

We apply our method *L2I* on a Multiple Sclerosis dataset, where multi-site MR images are used to train a binary classification network to distinguish between MS patients and healthy subjects. Due to the scanner bias in the images, a vanilla classification network and its variations show a weak performance. Also classical domain adaptation and contrastive learning methods cannot significantly improve the results. *L2I* strongly outperforms state-of-the-art methods in this setup. As the main task is performed only using disease-related features, this improves the generalization ability of the model. Medical images acquired with different scanners are a common scenario in long-term or multi-center studies. Our method shows a major improvement for this scenario compared to state-of-the-art methods.

Experiments on a multi-class dataset would be interesting, if an adequate dataset would be at hand. The proposed method can be applied to non-medical datasets for domain adaption. For future work, we will apply this idea to more complex tasks such as image segmentation or anomaly detection.

## References

Ackaouy, A.; Courty, N.; Vallée, E.; Commowick, O.; Barillot, C.; and Galassi, F. 2020. Unsupervised domain adaptation with optimal transport in multi-site segmentation of multiple sclerosis lesions from MRI data. *Frontiers in computational neuroscience*, 14: 19.

Ben-David, S.; Blitzer, J.; Crammer, K.; Kulesza, A.; Pereira, F.; and Vaughan, J. W. 2010. A theory of learning from different domains. *Machine learning*, 79(1): 151–175.

Billot, B.; Greve, D.; Van Leemput, K.; Fischl, B.; Iglesias, J. E.; and Dalca, A. V. 2020. A Learning Strategy for Contrast-agnostic MRI Segmentation. *arXiv preprint arXiv:2003.01995*.

Chaitanya, K.; Erdil, E.; Karani, N.; and Konukoglu, E. 2020. Contrastive learning of global and local features for medical image segmentation with limited annotations. *arXiv preprint arXiv:2006.10511*.

Chartsias, A.; Joyce, T.; Papanastasiou, G.; Semple, S.; Williams, M.; Newby, D. E.; Dharmakumar, R.; and Tsafaris, S. A. 2019. Disentangled representation learning in cardiac image analysis. *Medical image analysis*, 58: 101535.

Cohen, J. 1960. A coefficient of agreement for nominal scales. *Educational and Psychological Measurement*, 20(1): 37–46.

Dewey, B. E.; Zhao, C.; Reinholt, J. C.; Carass, A.; Fitzgerald, K. C.; Sotirchos, E. S.; Saidha, S.; Oh, J.; Pham, D. L.; Calabresi, P. A.; et al. 2019. DeepHarmony: a deep learning approach to contrast harmonization across scanner changes. *Magnetic resonance imaging*, 64: 160–170.

Dewey, B. E.; Zuo, L.; Carass, A.; He, Y.; Liu, Y.; Mowry, E. M.; Newsome, S.; Oh, J.; Calabresi, P. A.; and Prince, J. L. 2020. A Disentangled Latent Space for Cross-Site MRI Harmonization. In *International Conference on Medical Image Computing and Computer-Assisted Intervention*, 720–729. Springer.

Dinsdale, N. K.; Jenkinson, M.; and Namburete, A. I. 2020. Unlearning Scanner Bias for MRI Harmonisation. In *International Conference on Medical Image Computing and Computer-Assisted Intervention*, 369–378. Springer.

Dou, Q.; Castro, D. C.; Kamnitsas, K.; and Glocker, B. 2019. Domain generalization via model-agnostic learning of semantic features. *arXiv preprint arXiv:1910.13580*.

Ganin, Y.; Ustinova, E.; Ajakan, H.; Germain, P.; Larochelle, H.; Laviolette, F.; Marchand, M.; and Lempitsky, V. 2016. Domain-Adversarial Training of Neural Networks. *J. Mach. Learn. Res.*, 17(1): 2096–2030.

Hadsell, R.; Chopra, S.; and LeCun, Y. 2006. Dimensionality reduction by learning an invariant mapping. In *2006 IEEE Computer Society Conference on Computer Vision and Pattern Recognition*, volume 2, 1735–1742.

Hanley, J. A.; and McNeil, B. J. 1982. The meaning and use of the area under a receiver operating characteristic (ROC) curve. *Radiology*, 143(1): 29–36.

Harms, M. P.; Somerville, L. H.; Ances, B. M.; Andersson, J.; Barch, D. M.; Bastiani, M.; Bookheimer, S. Y.; Brown, T. B.; Buckner, R. L.; Burgess, G. C.; et al. 2018. Extending the Human Connectome Project across ages: Imaging protocols for the Lifespan Development and Aging projects. *NeuroImage*, 183: 972–984.

Hinterreiter, A.; Streit, M.; and Kainz, B. 2020. Projective Latent Interventions for Understanding and Fine-Tuning Classifiers. In *Interpretable and Annotation-Efficient Learning for Medical Image Computing*, 13–22. Springer.

Hosseini-Asl, E.; Keynton, R.; and El-Baz, A. 2016. Alzheimer’s disease diagnostics by adaptation of 3D convolutional network. In *2016 IEEE International Conference on Image Processing*, 126–130.

Huang, S.-W.; Lin, C.-T.; Chen, S.-P.; Wu, Y.-Y.; Hsu, P.-H.; and Lai, S.-H. 2018. AugGAN: Cross domain adaptation with GAN-based data augmentation. In *Proceedings of the European Conference on Computer Vision*, 718–731.

Isensee, F.; Schell, M.; Pflueger, I.; Brugnara, G.; Bonekamp, D.; Neuberger, U.; Wick, A.; Schlemmer, H.-P.; Heiland, S.; Wick, W.; et al. 2019. Automated brain extraction of multisequence MRI using artificial neural networks. *Human brain mapping*, 40(17): 4952–4964.

Kamnitsas, K.; Baumgartner, C.; Ledig, C.; Newcombe, V.; Simpson, J.; Kane, A.; Menon, D.; Nori, A.; Criminisi, A.; Rueckert, D.; et al. 2017. Unsupervised domain adaptation in brain lesion segmentation with adversarial networks. In *International conference on information processing in medical imaging*, 597–609. Springer.

Kang, G.; Jiang, L.; Yang, Y.; and Hauptmann, A. G. 2019. Contrastive adaptation network for unsupervised domain adaptation. In *Proceedings of the IEEE Conference on Computer Vision and Pattern Recognition*, 4893–4902.

Kaur, B.; Lemaître, P.; Mehta, R.; Sepahvand, N. M.; Precup, D.; Arnold, D.; and Arbel, T. 2019. Improving pathological structure segmentation via transfer learning across diseases. In *Domain Adaptation and Representation Transfer and Medical Image Learning with Less Labels and Imperfect Data*, 90–98. Springer.

Khosla, P.; Teterwak, P.; Wang, C.; Sarna, A.; Tian, Y.; Isola, P.; Maschinot, A.; Liu, C.; and Krishnan, D. 2020. Supervised contrastive learning. *arXiv preprint arXiv:2004.11362*.

Kingma, D. P.; and Ba, J. 2014. Adam: A method for stochastic optimization. *arXiv preprint arXiv:1412.6980*.

Kushibar, K.; Valverde, S.; González-Villà, S.; Bernal, J.; Cabezas, M.; Oliver, A.; and Lladó, X. 2019. Supervised domain adaptation for automatic sub-cortical brain structure segmentation with minimal user interaction. *Scientific reports*, 9(1): 1–15.

Lei, Y.; Wang, T.; Liu, Y.; Higgins, K.; Tian, S.; Liu, T.; Mao, H.; Shim, H.; Curran, W. J.; Shu, H.-K.; et al. 2019. MRI-based synthetic CT generation using deep convolutional neural network. In *Medical Imaging 2019: Image*

*Processing*, volume 10949, 109492T. International Society for Optics and Photonics.

Ma, Q.; Zhang, T.; Zanetti, M. V.; Shen, H.; Satterthwaite, T. D.; Wolf, D. H.; Gur, R. E.; Fan, Y.; Hu, D.; Busatto, G. F.; et al. 2018. Classification of multi-site MR images in the presence of heterogeneity using multi-task learning. *NeuroImage: Clinical*, 19: 476–486.

Motian, S.; Piccirilli, M.; Adjerooh, D. A.; and Doretto, G. 2017. Unified deep supervised domain adaptation and generalization. In *Proceedings of the IEEE international conference on computer vision*, 5715–5725.

Novosad, P.; Fonov, V.; and Collins, D. L. 2019. Unsupervised domain adaptation for the automated segmentation of neuroanatomy in MRI: a deep learning approach. *bioRxiv*, 845537.

Oord, A. v. d.; Li, Y.; and Vinyals, O. 2018. Representation learning with contrastive predictive coding. *arXiv preprint arXiv:1807.03748*.

Park, C.; Lee, J.; Yoo, J.; Hur, M.; and Yoon, S. 2020. Joint Contrastive Learning for Unsupervised Domain Adaptation. *arXiv preprint arXiv:2006.10297*.

Perone, C. S.; Ballester, P.; Barros, R. C.; and Cohen-Adad, J. 2019. Unsupervised domain adaptation for medical imaging segmentation with self-ensembling. *NeuroImage*, 194: 1–11.

Rozantsev, A.; Salzmann, M.; and Fua, P. 2018. Residual parameter transfer for deep domain adaptation. In *Proceedings of the IEEE Conference on Computer Vision and Pattern Recognition*, 4339–4348.

Saenko, K.; Kulis, B.; Fritz, M.; and Darrell, T. 2010. Adapting visual category models to new domains. In *European conference on computer vision*, 213–226. Springer.

Sankaranarayanan, S.; Balaji, Y.; Castillo, C. D.; and Chellappa, R. 2018. Generate to adapt: Aligning domains using generative adversarial networks. In *Proceedings of the IEEE Conference on Computer Vision and Pattern Recognition*, 8503–8512.

Schroff, F.; Kalenichenko, D.; and Philbin, J. 2015. Facenet: A unified embedding for face recognition and clustering. In *Proceedings of the IEEE conference on computer vision and pattern recognition*, 815–823.

Szegedy, C.; Ioffe, S.; Vanhoucke, V.; and Alemi, A. 2017. Inception-v4, inception-resnet and the impact of residual connections on learning. In *Proceedings of the AAAI Conference on Artificial Intelligence*, volume 31.

Tustison, N. J.; Avants, B. B.; Cook, P. A.; Zheng, Y.; Egan, A.; Yushkevich, P. A.; and Gee, J. C. 2010. N4ITK: improved N3 bias correction. *IEEE transactions on medical imaging*, 29(6): 1310–1320.

Tzeng, E.; Hoffman, J.; Darrell, T.; and Saenko, K. 2015. Simultaneous deep transfer across domains and tasks. In *Proceedings of the IEEE international conference on computer vision*, 4068–4076.

Tzeng, E.; Hoffman, J.; Saenko, K.; and Darrell, T. 2017. Adversarial discriminative domain adaptation. In *Proceedings of the IEEE conference on computer vision and pattern recognition*, 7167–7176.

Valverde, S.; Salem, M.; Cabezas, M.; Pareto, D.; Vilanova, J. C.; Ramió-Torrentà, L.; Rovira, À.; Salvi, J.; Oliver, A.; and Lladó, X. 2019. One-shot domain adaptation in multiple sclerosis lesion segmentation using convolutional neural networks. *NeuroImage: Clinical*, 21: 101638.

Van Essen, D. C.; Ugurbil, K.; Auerbach, E.; Barch, D.; Behrens, T. E.; Bucholz, R.; Chang, A.; Chen, L.; Corbetta, M.; Curtiss, S. W.; et al. 2012. The Human Connectome Project: a data acquisition perspective. *NeuroImage*, 62(4): 2222–2231.

Wang, S.; Zhang, L.; and Fu, J. 2020. Adversarial transfer learning for cross-domain visual recognition. *Knowledge-Based Systems*, 204: 106258.

Wen, G.; Chen, H.; Cai, D.; and He, X. 2018. Improving face recognition with domain adaptation. *Neurocomputing*, 287: 45–51.

Wen, Y.; Zhang, K.; Li, Z.; and Qiao, Y. 2016. A discriminative feature learning approach for deep face recognition. In *European conference on computer vision*, 499–515. Springer.

Wolterink, J. M.; Dinkla, A. M.; Savenije, M. H.; Seevinck, P. R.; van den Berg, C. A.; and Işgum, I. 2017. Deep MR to CT synthesis using unpaired data. In *International workshop on simulation and synthesis in medical imaging*, 14–23. Springer.

Zhang, Y.; David, P.; and Gong, B. 2017. Curriculum domain adaptation for semantic segmentation of urban scenes. In *Proceedings of the IEEE International Conference on Computer Vision*, 2020–2030.

# Learn to Ignore: Domain Adaptation for Multi-Site MRI Analysis

## – Technical Appendix –

### 1 Office31 as Baseline Dataset for Domain Adaptation

To compare the performance of the proposed method  $L2I$  to state-of-the-art algorithms on a classical domain adaptation problem, we use the Office31 dataset (Saenko et al. 2010). Out of its 31 classes, we select mobile phones and speakers for our experiment of binary classification. As source domain, we choose the *Amazon* dataset, where the images are taken from the Amazon webshop. The images of the *Webcam* dataset were acquired using a webcam and form the target domain. All input images  $x_i \in \mathbb{R}^2$  are of size (3, 256, 256), four examples are shown in Figure 1. The split into training, validation and test set is summarized in Table 2. The same architecture and method is used as described in the main paper in Figure 2, with the only difference being the 2D instead of 3D convolutions in the Encoder  $E$ . This results in a total number of 24 502 242 parameters for 2D input data.



Figure 1: Exemplary images of the Office31 dataset for both domains *Amazon* and *Webcam*, as well as for both classes *mobile phone* and *speaker*.

We want to point out that both the *Amazon* and the *Webcam* dataset provide images of both classes. The data allocation is visualized in the quantity chart in Figure 2. In contrast to the problem of the MS dataset, here no features related to the provenance of the images can be taken to distinguish between the classes on the source domain. Therefore, the main

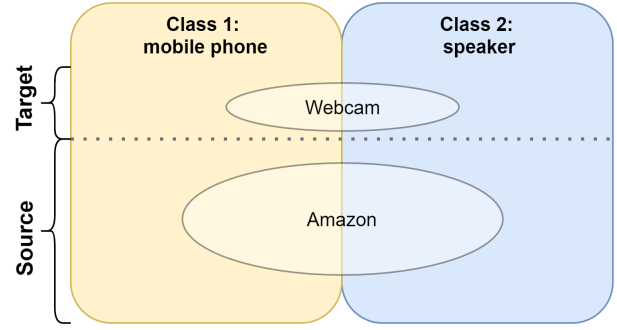


Figure 2: Quantity chart for the source and target domain of the Office31 dataset. Both the *Amazon* and the *Webcam* dataset provide images of both classes.

task can be learned on the source domain, and the model has to overcome the domain shift between the source and the target domain. Consequently, this is a classical domain adaptation task, which can be tackled with classical domain adaptation algorithms. The problem on the MS dataset presented in Figure 4 in the main paper is therefore substantially different from this task. We want to demonstrate that although our method was specifically designed to solve the problem presented in the main paper, it is still able to solve a classical domain adaptation task. We evaluate all methods for 10 different random train-validation-test splits according to Table 2.

	ACC	KAPPA	AUROC
VANILLA	70.5 [6.0]	41.0 [12.0]	78.6 [11.7]
· CLASS-AWARE	77.0 [6.7]	54.0 [13.5]	89.9 [3.3]
· WEIGHTED	76.0 [6.1]	52.0 [12.3]	87.6 [8.6]

Table 1: Mean and standard deviation of the classification results for the *Vanilla*, *Class-aware* and *Weighted* methods when trained only on the target domain for 10 runs.

In Table 1, the classification results (mean [standard deviation]) of the 10 runs when trained only on the target domain are presented. Training on such a small dataset leads to over-

		TRAINING SET		VALIDATION SET		TEST SET	
		MOBILE PHONE	SPEAKER	MOBILE PHONE	SPEAKER	MOBILE PHONE	SPEAKER
TARGET	WEBCAM	12	12	8	8	10	10
SOURCE	AMAZON	82	81	8	8	10	10

Table 2: Overview of the split into training, validation and test set for the Office31 dataset.

	ACC	TARGET	AUROC	SOURCE		
		KAPPA		ACC	KAPPA	AUROC
VANILLA	74.5 [9.0]	49.0 [17.9]	80.0 [17.1]	92.0 [5.4]	84.0 [10.7]	96.6 [4.5]
· CLASS-AWARE	77.0 [10.9]	54.0 [21.7]	78.9 [15.9]	93.0 [4.2]	86.0 [8.4]	95.2 [4.5]
· WEIGHTED	78.5 [9.7]	57.0 [19.4]	88.5 [12.4]	91.0 [7.0]	83.0 [13.4]	95.1 [6.1]
DANN	87.5 [7.2]	75.0 [14.3]	92.6 [6.7]	93.5 [5.8]	86.0 [10.7]	97.0 [6.1]
UNLEARNING	92.0 [4.8]	94.0 [9.7]	97.9 [4.0]	<b>99.0 [2.1]</b>	<b>98.0 [4.2]</b>	<b>100.0 [0.0]</b>
CONTRASTIVE	85.5 [8.6]	71.0 [17.3]	95.4 [4.5]	91.0 [8.8]	82.0 [17.5]	99.7 [0.7]
CAN	<b>94.0 [7.7]</b>	<b>88.0 [15.5]</b>	<b>99.9 [0.3]</b>	97.0 [3.5]	94.0 [7.0]	99.8 [0.6]
L2I [OURS]	92.5 [4.1]	84.0 [9.7]	96.4 [4.0]	92.0 [6.7]	84.0 [13.5]	96.7 [4.1]
· FIXED	90.5 [6.9]	81.0 [13.7]	80.9 [7.4]	86.0 [8.4]	72.0 [16.9]	83.3 [10.9]
· NO-MARGIN	90.0 [4.6]	80.0 [9.3]	91.2 [8.5]	89.5 [6.9]	79.0 [13.7]	90.7 [11.6]

Table 3: Mean and standard deviation of the classification results on the Office31 test set for 10 runs. Our method *L2I* achieves results similar to state-of-the-art methods.

fitting and a poor classification performance on the test set. Therefore, the target domain is complemented with images from the source domain. Like in the main paper, the results for training on both the source and the target domain for 10 runs are shown in Table 3.

When comparing *L2I* against the other methods on the Office31 dataset, we see that *L2I* has a similar performance as state-of-the-art domain adaptation and contrastive-learning methods. All methods achieve good results on the source domain. We observe that the *Vanilla* classifier performs worse on the target domain compared to the source domain. This indicates that the model is not able to overcome the domain shift between the source and the target domain. The small amount of data leads to huge jumps in the accuracy scores when images are classified differently, and consequently to large values for the standard deviation.

The state-of-the-art domain adaptation methods *CAN* and *Unlearning* achieve very good results, followed by *DANN* and *Contrastive*. Our method *L2I* achieves similar results as those methods. Moreover, we see that class-aware sampling and weighting the loss improves the classification performance compared to the *Vanilla* classifier, but does not reach the level of the other methods. On this dataset, *Fixed* also achieves good results. With those experiments, we could show that *L2I* is able to achieve good results on a classical domain adaptation problem, although it was designed for the specific problem setup presented in the main paper.

## 2 Study Details of the MS Dataset

In Table 4 we give more details about the different datasets presented in Figure 4 of the main paper. All mentioned scanner models are 3T Siemens scanners. The column *Gender*

indicates the number of male and female subjects, whereas the column *Age* gives the minimal and maximal age of the subjects in the respective studies.

	Scanner Model	Age	Gender [m / f]
ADNI	Trio Trim	56-78	54 / 74
HCP	Connectome Skyra	22-35	49 / 51
HCPA	Prisma	36-88	66 / 91
Study 1	Trio Trim	19-62	34 / 58
Study 2	Skyra-fit, Skyra	20-76	137 / 279
Study 3	Skyra	27-78	21 / 31
Study 4	Skyra	21-47	12 / 12
Study 5	Trio Trim	26-55	4 / 5

Table 4: Details about the scanner type, age and gender distribution for the studies used in this paper.

## 3 T-SNE Plots

We show a t-SNE plot of the latent vectors of the validation and test set. We distinguish between healthy and diseased subjects, and the affiliation to the source or target dataset. In Figure 3 we present the results when using the *Vanilla* classifier. We can identify two clusters of the source domain, separating healthy from diseased subjects. However the latent vectors of the target domain cannot be easily distinguished. In Figure 4, the t-SNE plot is shown for our method *L2I*. Except for some datapoints that were grouped incorrectly, we can distinguish between healthy and diseased subjects, regardless of their affiliation to the source or target domain.

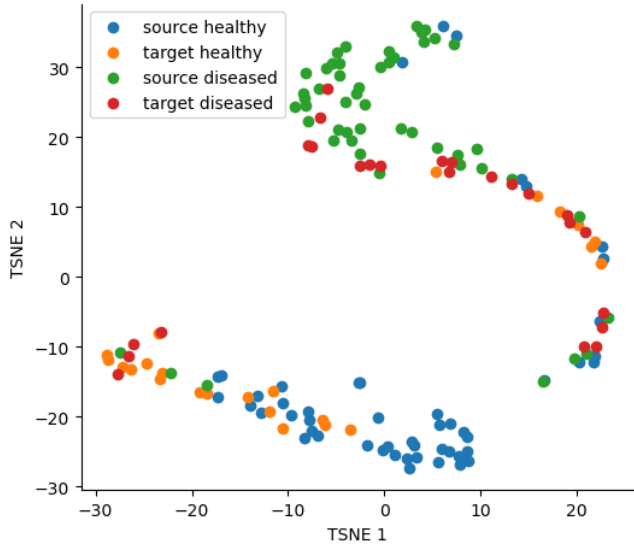


Figure 3: T-SNE plot of the latent vectors using the *Vanilla* classifier. On the target domain (orange and red data-points), the distinction between healthy and diseased subjects cannot clearly be seen.

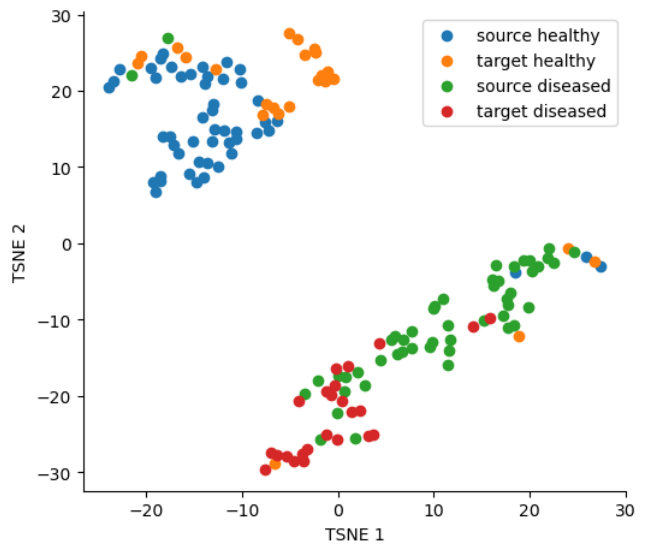


Figure 4: T-SNE plot of the latent vectors using *L2I*. The separation between healthy and diseased subjects can be seen.

## References

Saenko, K.; Kulis, B.; Fritz, M.; and Darrell, T. 2010. Adapting visual category models to new domains. In *European conference on computer vision*, 213–226. Springer.